Cannabinoid receptor 1-expressing neurons in the nucleus accumbens

Bradley D. Winters[a,1], Juliane M. Krüger[b,1,2], Xiaojie Huang[b], Zachary R. Gallaher[a], Masago Ishikawa[c], Krzysztof Czaja[a], James M. Krueger[a], Yanhua H. Huang[a,c], Oliver M. Schlüter[b,d,3], and Yan Dong[a,e,3]

[a]Program in Neuroscience, Washington State University, Pullman, WA 99164; [b]Molecular Neurobiology, European Neuroscience Institute, 37077 Göttingen, Germany; Departments of [c]Psychiatry and [e]Neuroscience, University of Pittsburgh, Pittsburgh, PA 15260; and [d]Cluster of Excellence "Nanoscale Microscopy and Molecular Physiology of the Brain" (CNMPB), European Neuroscience Institute, 37077 Göttingen, Germany

Edited* by Robert C. Malenka, Stanford University School of Medicine, Stanford, CA, and approved August 16, 2012 (received for review April 17, 2012)

Endocannabinoid signaling critically regulates emotional and motivational states via activation of cannabinoid receptor 1 (CB1) in the brain. The nucleus accumbens (NAc) functions to gate emotional and motivational responses. Although expression of CB1 in the NAc is low, manipulation of CB1 signaling within the NAc triggers robust emotional/motivational alterations related to drug addiction and other psychiatric disorders, and these effects cannot be exclusively attributed to CB1 located at afferents to the NAc. Rather, CB1-expressing neurons in the NAc, although sparse, appear to be critical for emotional and motivational responses. However, the cellular properties of these neurons remain largely unknown. Here, we generated a knock-in mouse line in which CB1-expressing neurons expressed the fluorescent protein td-Tomato (tdT). Using these mice, we demonstrated that tdT-positive neurons within the NAc were exclusively fast-spiking interneurons (FSIs). These FSIs were electrically coupled with each other, and thus may help synchronize populations/ensembles of NAc neurons. CB1-expressing FSIs also form GABAergic synapses on adjacent medium spiny neurons (MSNs), providing feed-forward inhibition of NAc output. Furthermore, the membrane excitability of tdT-positive FSIs in the NAc was up-regulated after withdrawal from cocaine exposure, an effect that might increase FSI-to-MSN inhibition. Taken together with our previous findings that the membrane excitability of NAc MSNs is decreased during cocaine withdrawal, the present findings suggest that the basal functional output of the NAc is inhibited during cocaine withdrawal by multiple mechanisms. As such, CB1-expressing FSIs are targeted by cocaine exposure to influence the overall functional output of the NAc.

Cannabinoid receptor type 1 (CB1) has been extensively implicated in a variety of psychological and psychiatric disorders, including drug addiction (1, 2). Recent studies suggest that CB1 within the nucleus accumbens (NAc), a key component of the brain reward circuit, plays a particularly important role in the development and maintenance of cocaine-induced behavioral alterations (3). Compared with the extensive expression of CB1 in the striatum, the mRNA and protein levels of CB1 within the NAc are sparse, leading to the notion that CB1 at afferent terminals projecting to the NAc are largely responsible for intra-NAc, CB1-dependent, cocaine-induced behaviors (4–6). However, a recent study primarily targeting CB1-expressing neurons demonstrates that inhibiting the expression of CB1 within the NAc antagonizes cocaine-induced reward responses (7). This and other results (8) suggest that CB1-expressing neurons in the NAc, although sparse, are critical for cellular and behavioral alterations induced by cocaine and other drugs of abuse.

To examine these putative CB1-expressing neurons within the NAc, we generated a knock-in mouse line in which CB1-expressing neurons expressed the fluorescent protein td-Tomato (tdT). Our results show that tdT-positive neurons within the NAc were exclusively fast-spiking interneurons (FSIs). These FSIs were not only electrically connected with each other but exerted extensive inhibitory control on nearby medium spiny neurons (MSNs), the principal neurons in the NAc, via monosynaptic connections. Furthermore, the membrane excitability of these neurons became significantly up-regulated throughout short- and long-term withdrawal from repeated exposure to cocaine. These results suggest that CB1-expressing FSIs within the NAc are neural substrates targeted by cocaine exposure and influence the overall functional output of the NAc.

Results

Labeling CB1-Expressing Neurons. To label CB1-expressing neurons genetically, we generated a bicistronic gene for CB1 with tdT expressed after an internal ribosome entry site (IRES) element (Fig. 1*A*). With an IRES, soluble fluorophore was expressed under the control of endogenous CB1 promoter but did not physically attach to CB1. Thus, expression of CB1 should not be affected in this mouse model. Western blot analysis showed that the brain expression of CB1 was similar between WT and CB1-tdT mice (WT: 100.0 ± 4.7, $n = 3$; tdT: 95.4 ± 11.0, $n = 3$; $P = 0.75$, t test; Fig. 1*A*).

To examine whether tdT signals were sufficient for detection of CB1-expressing neurons, we imaged tdT-expressing neurons in both thin (30 μm) and thick (180 μm) brain slices without immunostaining. Note that the tdT signal in the soma is a cellular marker and the actual CB1 is probably only on presynaptic terminals. Nonetheless, our results showed that the distribution patterns of tdT-positive neurons and neuronal processes ($n = 7$ mice) were highly consistent with that of CB1 characterized in previous studies using immunostaining, in situ hybridization, and radioligand binding assays. Specifically, the cortical expression of tdT exhibited a clear laminar pattern with lower fiber and somatic expression in layer 4 and higher expression in layers 2/3 and 5 (Fig. 1 *B–E* and Fig. S1). Low expression was observed in layer 4 of the somatosensory cortex (9), corresponding to the whisker barrels (Fig. 1*C*). Cells with somatic expression of tdT were scattered in all layers and exhibited a range of sizes, expression levels, and morphology. Many cells with high somatic expression exhibited bi- or multipolar dendritic morphology consistent with interneurons. Neurons with pyramidal shapes also exhibited expression of tdT, but at a very low level (Fig. S1).

Author contributions: B.D.W., J.M. Krüger, J.M. Krueger, Y.H.H., O.M.S., and Y.D. designed research; B.D.W., J.M. Krüger, X.H., and Z.R.G. performed research; K.C. contributed new reagents/analytic tools; B.D.W., J.M. Krüger, X.H., and M.I. analyzed data; and B.D.W., O.M.S., and Y.D. wrote the paper.

The authors declare no conflict of interest.

*This Direct Submission article had a prearranged editor.

[1]B.D.W. and J.M.K. contributed equally to this work.

[2]Present address: Roche Pharma Research and Early Development, 82377 Penzberg, Germany.

[3]To whom correspondence may be addressed. E-mail: oschlue@gwdg.de or yandong@pitt.edu.

This article contains supporting information online at www.pnas.org/lookup/suppl/doi:10.1073/pnas.1206303109/-/DCSupplemental.

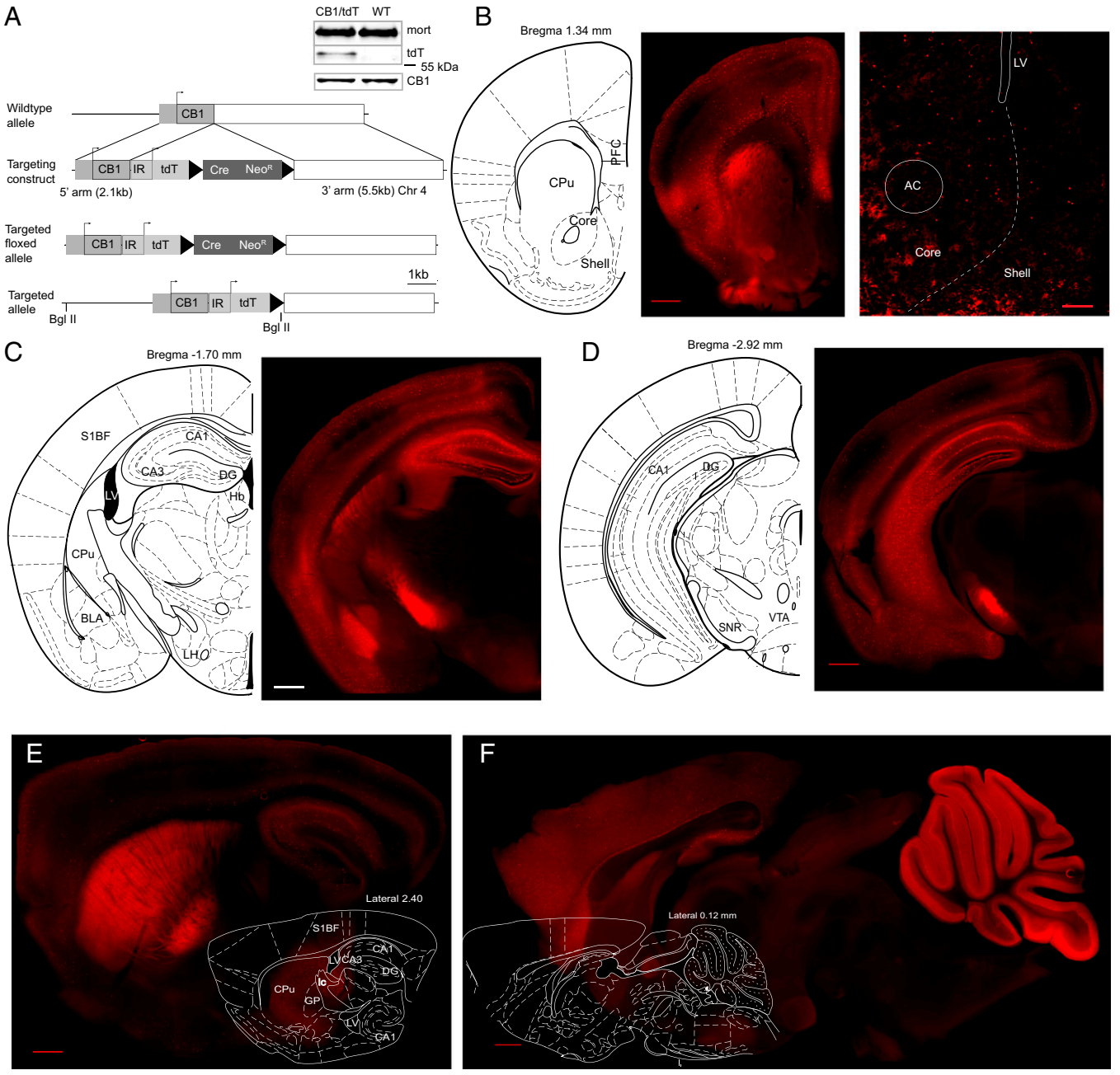

Fig. 1. Genetic labeling of CB1. (*A*) Diagram shows the constructs used to insert tdT and IRES (IR) in the CB1 gene. Western blot shows that the brain expression of CB1 was similar between WT and CB1/tdT transgenic mice relative to loading control mortalin (mort). (*B*) Example coronal section shows the expression pattern of tdT-positive cells in the prefrontal cortex (PFC), striatum, and NAc (*Left*) and a higher magnification of the NAc (*Right*). AC, anterior commissure; CPu, caudate/putamen; LV, lateral ventricle. (Scale bars: *Left*, 500 μm; *Right*, 200 μm.). (*C*) Example coronal section shows the expression pattern of tdT-positive cells in the cortex, amygdala, and hippocampus. BLA, basolateral amygdala; DG, dentate gyrus; LH, lateral hypothalamus; S1BF, S1 barrel field. (*D*) Example coronal section shows the expression pattern of tdT-positive cells in the cortex, hippocampus, and substantia nigra (SNR). (*E*) Example sagittal section shows extensive expression of tdT in cell bodies and fibers within the striatum and globus pallidus (GP). BMA, basomedial amygdala. (*F*) Example sagittal section shows extensive expression of tdT in the cerebellum. All images were obtained without immunostaining in 180-μm-thick sections (except *B*, *Right*, which was a 30 μm section). (Scale bars: *C*–*F*, 500 μm.) Atlas panels modified with permission from ref. 55. Images showing whole brain sections in *B*–*F* were produced from montages of higher-magnification images stitched together.

These findings are consistent with previous studies using different experimental approaches in cortices (4, 5, 10–14). The medial prefrontal cortex (mPFC) exhibited higher expression of tdT than adjacent cortical regions (Fig. 1*B*), consistent with the expression pattern of previous results (4). In addition, we observed expression of tdT in both cell bodies and fibers in layer 1 of cortex. This observation is different from some reports (14, 15) but consistent with others (10) about CB1 expression in the cortex.

The expression pattern of tdT in the basal ganglia was similar to previous reports of CB1 expression (4, 5, 10–14). In the caudate/putamen, there was a clear dorsolateral-to-ventromedial decrease in expression, with virtually all medium-sized neurons in the dorsolateral region exhibiting somatic expression (Fig. 1 *B*,

C, and *E*). In contrast, the NAc exhibited relatively low expression of tdT, consistent with the expression pattern of CB1 reported previously (10–12). These NAc tdT-positive neurons were medium-sized and sparsely distributed, with clear tdT-positive neuronal fibers (Fig. 1*B*). In addition, these tdT-positive neurons were not seemingly anatomically clustered (11) but, instead, evenly distributed in both the NAc core and shell (Fig. 1*B*). In the midbrain, expression of tdT was high in portions of the substantia nigra (Fig. 1 *C* and *D*) and limited to axonal fibers, with no somatic expression observed. Consistent with previous results of CB1 expression (4, 10, 11), no somatic expression of tdT and minimal fiber expression of tdT were observed in the ventral tegmental area (VTA) (Fig. 1*D* and Fig. S1).

The habenula exhibited very low expression of tdT (Fig. 1*C*). In the hippocampus, sparse high somatic expression of tdT was observed in the regions outside the pyramidal cell layers of the hippocampus, and large numbers of fluorescent fibers were present surrounding the pyramidal cells (Fig. 1 *C*–*E*). These observations are consistent with previous results of CB1 expression (4, 5, 11, 13). In the cerebellum, where CB1 is extensively expressed (4, 10, 16), high expression of tdT was detected (Fig. 1*F*).

Collectively, our results suggest that CB1-expressing neurons were faithfully labeled with tdT in this mouse line.

tdT-Positive Cells in the NAc Are FSIs. To characterize the electrophysiological properties of CB1-expressing neurons in the NAc, we targeted these neurons based on their tdT signals (Fig. 2*A*) and performed whole-cell current-clamp recordings. Compared with principal MSNs, these tdT-positive neurons (n = 57) exhibited a high maximal rate of evoked action potential (AP) firing, short AP half-width, large afterhyperpolarization potential, and little inward rectification (Fig. 2 *B*–*G* and Table S1). These membrane properties are consistent with those of FSIs previously reported in the striatum and NAc (17–19), and they are distinctively different from those of MSNs or other types of interneurons that have been characterized in the striatum and NAc (18, 20–24). Indeed, all tdT-positive neurons (n = 327) recorded throughout the study exhibited the fast-spiking properties, suggesting that (*i*) CB1-expressing NAc neurons were exclusively FSIs and, as such, (*ii*) NAc MSNs did not express CB1.

Using immunostaining approaches, we next attempted to verify these conclusions and to explore the biochemical properties of NAc tdT-expressing neurons. Thus far, three major types of medium-sized GABAergic interneurons have been identified in the striatum based on the differential expression of their signature proteins: (*i*) parvalbumin (PV), (*ii*) calretinin (CR), and (*iii*) somatostatin or neuropeptide Y or nitric oxide synthase (SOM/NPY/NOS) (21). Expression of PV can serve as a reliable marker for FSIs, because all striatal PV-expressing interneurons that have been recorded thus far are FSIs (18, 19, 22). We thus examined whether tdT-expressing FSIs in the NAc were indeed PV-expressing FSIs by dual immunostaining for tdT (using dsRed antibody) and PV in coronal slices from CB1-tdT mice (n = 5). Within the NAc shell and core, 52% of tdT-positive cells (total of 541 cells) were also labeled with PV, whereas 65% of PV-positive cells (total of 437 cells) were colabeled with tdT (Fig. 3 *A*–*D* and *SI Results*). The partial overlap of tdT- and PV-expressing neurons suggests that at least three types of FSIs are present in the NAc: (*i*) FSIs expressing CB1 only, (*ii*) FSIs expressing PV only, and (*iii*) FSIs expressing both CB1 and PV. In addition, both tdT- and PV-expressing neurons within the NAc exhibited a rostral-to-caudal decrease in the density, a distribution pattern in concert with previous mRNA-based results of CB1 expression (25). It is also worth noting that the colocalization of PV and CB1 is not observed in the somatosensory cortex (14) or hippocampus (26). Nonetheless, a remaining question is whether CB1-positive, PV-negative FSIs fall into any known neuronal subtypes. SOM/NPY/NOS-expressing interneurons can be largely excluded due to their distinct electrophysiological and morphological properties (18, 22, 27–30). CR-expressing neurons, however, remained unchecked for their electrophysiological properties. Using triple immunostaining in coronal slices from CB1-tdT mice (n = 3), we observed strong and extensive CR signals in neuronal processes in the NAc shell, with very few CR-positive somas, as reported previously (31). Furthermore, very few CR-positive cells are tdT-positive (4 of

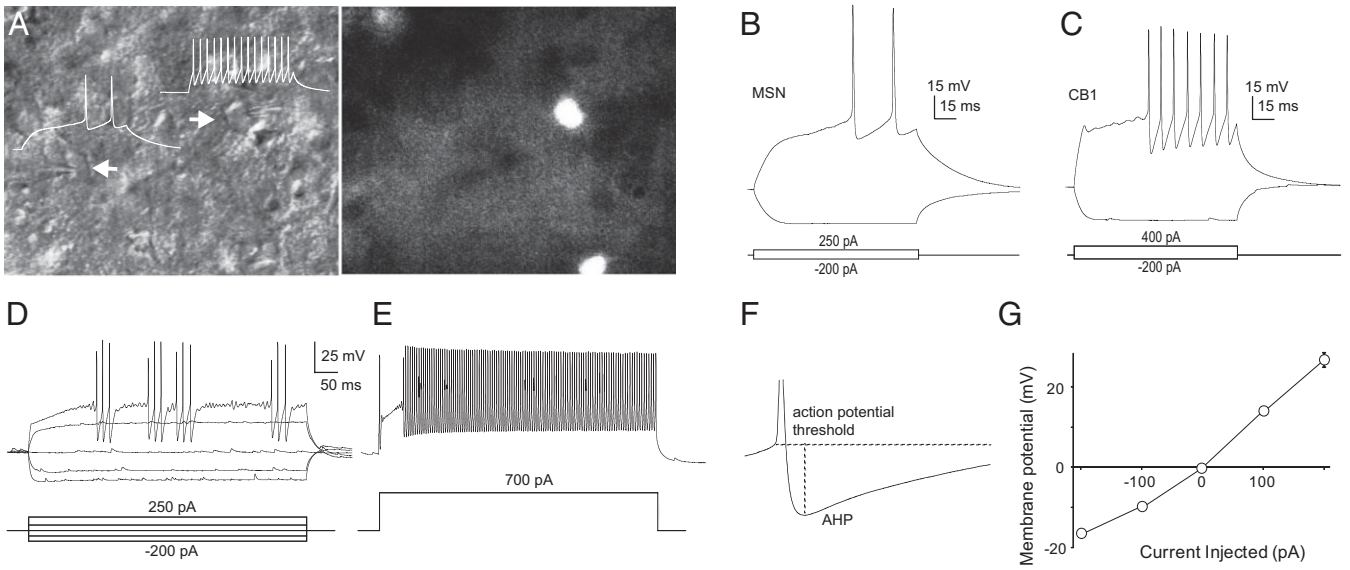

Fig. 2. CB1-expressing neurons in the NAc are FSIs. (*A*) Example images show dual recordings (*Left*) from an MSN (*Lower*) and an FSI (*Upper*) with or without tdT fluorescent signals (*Right*) in the NAc. Images were obtained using regular slice electrophysiology microscopy. Differential interference contrast (DIC) (*Left*), and the same slice but filtered for red fluorescence (*Right*). (*B*) Membrane properties of an example MSN in the NAc. (*C*) Membrane properties of an example FSI in the NAc. (*D*) Voltage traces from an example tdT-positive neuron exhibit a stuttering firing pattern. (*E*) Voltage traces from the same neuron shown in *D* exhibit a high-frequency firing pattern. (*F*) Voltage trace from an example tdT-positive neuron shows a large afterhyperpolarization potential (AHP). (*G*) Steady-state current-voltage (I-V) curve of tdT-positive neurons in the NAc (n = 23/6).

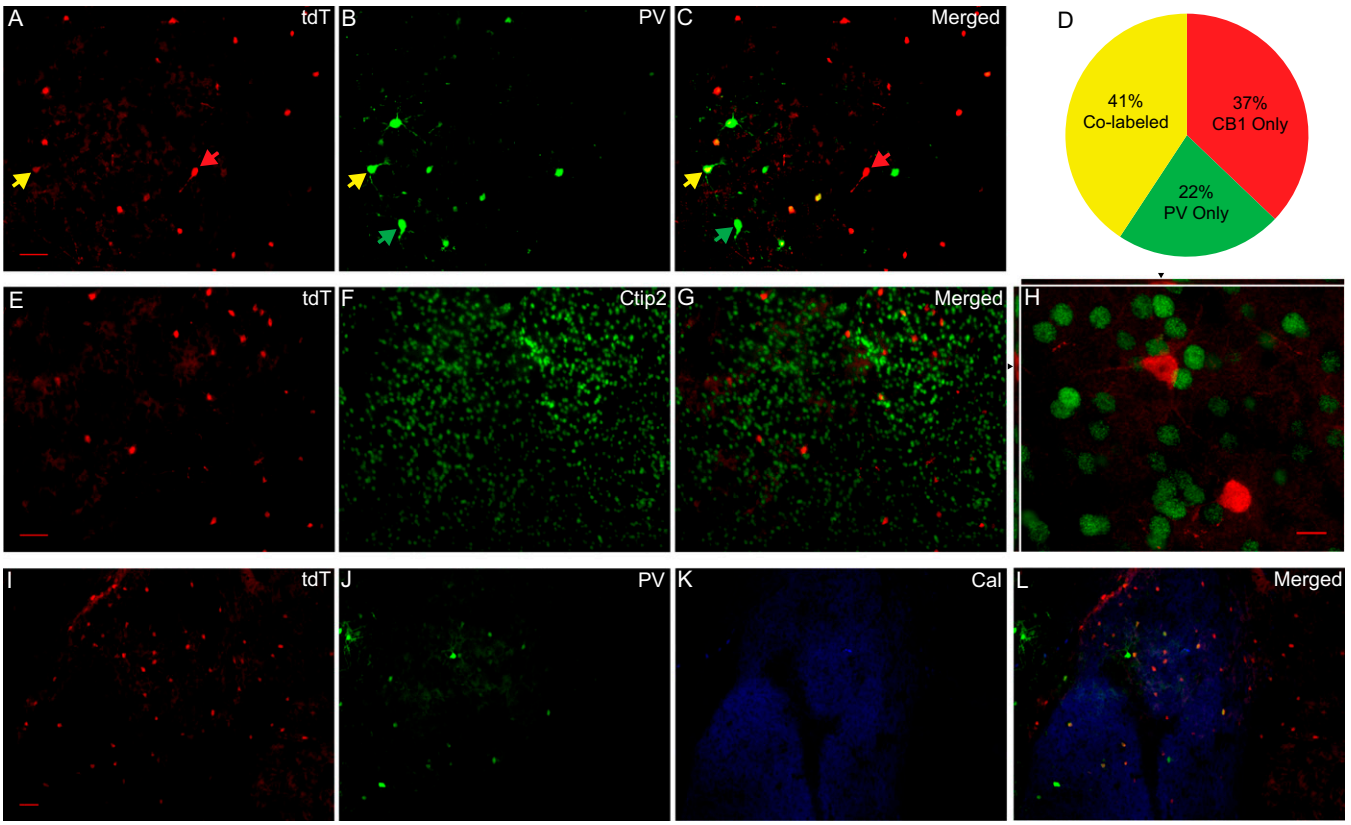

Fig. 3. Biochemical properties of CB1-expressing neurons in the NAc. (*A*) Image from an example brain slice shows tdT expression (red) in the NAc shell following immunostaining using the dsRed antibody. (Scale bar, 50 μm.) (*B*) Same slice used in *A* imaged for PV expression (green). (*C*) Merger of *A* and *B*. The tdT- and PV-coexpressing cells are labeled by yellow arrows, tdT-only cells by red arrows, and PV-only cell by green arrows. (*D*) Summary chart illustrates percentage of total neurons counted (n = 696) in the NAc core and shell for labeling of CB1 (tdT) and PV, and their partial overlap. (*E*) Image from an example NAc slice shows tdT expression (red) in the shell (by dsRed antibody). (Scale bar: 10 μm.) (*F*) Same slice used in *E* imaged for Ctip2 expression (green). (*G*) Merger of *E* and *F*. (*H*) Example high-magnification image shows Ctip2 (green) and tdT (red) in the NAc shell. The 3D panels on top and side show the focal depth the upper tdT-positive cell. (Scale bar: 10 μm.) (*I*) Example image shows tdT expression (red) in the NAc shell. (Scale bar: *I–L*, 50 μm.) (*J*) Same slice in used in *I* imaged for PV expression (green). (*K*) Same slice used in *I* imaged for CR (Cal) expression (blue). (*L*) Merger of *I–K*.

242, 2.0 ± 0.8%; Fig. 3 *I*, *K*, and *L*) or PV-positive (1 of 242, 0.5 ± 0.5%; Fig. 3 *J–L*). As such, the tdT-positive, PV-negative neurons may represent a distinct population of FSIs in the NAc.

For NAc/striatal MSNs, COUP TF1-interacting protein 2 (Ctip2) has been identified as a reliable molecular marker (32). In coronal slices from CB1-tdT mice (n = 3), our immunostaining results show minimal overlap of tdT and Ctip2 in NAc neurons (22 of 788, 2.8 ± 0.4%; Fig. 3 *E–H*). These results confirm our electrophysiological conclusion that little CB1 is expressed in NAc MSNs.

Synaptic Connections of tdT-Positive FSIs. Dual recordings in the NAc shell from our CB1-tdT mice (6–8 wk old) revealed that tdT-positive FSIs were electrically coupled. In this experiment, two adjacent (75–250 μm apart) tdT-positive neurons were simultaneously recorded, one (tdT-a) in current-clamp configuration and the other (tdT-b) in voltage-clamp configuration (Fig. 4*A*). Current injections into tdT-a induced temporally correlated changes in the membrane potential of tdT-b, and APs elicited in tdT-a were always accompanied by temporally correlated electrical current spikes [excitatory postsynaptic current (EPSC)] in tdT-b (Fig. 4 *B–D*). These simultaneous events suggest that tdT-positive FSIs are electrically connected, similar to FSIs in the striatum (19). In our recordings, the majority (20 of 32) of pairs exhibited such an electrical coupling.

The tdT-positive FSIs were also connected with each other by chemical synapses; an AP in tdT-a often triggered a postsynaptic chemical current [inhibitory postsynaptic current (IPSC)] in tdT-b in the majority (23 of 32) of recorded pairs, with a delay of 0.71 ± 0.05 ms (AP peak to initiation of the synaptic current, n = 23; Fig. 4*B*), suggesting a monosynaptic transmission via chemical synapses. Furthermore, these synaptic currents were completely inhibited by perfusion of picrotoxin (0.1 mM, n = 4), confirming they were IPSCs.

In these paired recordings, both tdT-positive FSIs presumably expressed CB1, which may regulate the chemical synapses between them. An important and sensitive CB1-dependent short-term synaptic regulation is depolarization-induced suppression of inhibition (DSI). However, DSI was not induced at tdT-to-tdT inhibitory synapses (10 s at 0 mV, inhibition: 7.36 ± 4.50%; P = 0.86; n = 17/8; Fig. 4*E*). This result cannot be explained by a lack of expression of CB1 at these synapses because these synapses were sensitive to CB1-selective agonist WIN 55212-2 [(R)-(+)-[2,3-Dihydro-5-methyl-3-(4-morpholinylmethyl)pyrrolo[1,2,3-de]-1,4-benzoxazin-6-yl]-1-naphthalenylmethanone mesylate; 5 μM; n = 6/4], the perfusion of which substantially inhibited this unitary synaptic transmission by 60.9 ± 8.0% (Fig. 4*F*). Furthermore, this inhibition was accompanied by an increase in the paired-pulse ratio (PPR; $P < 0.04$, t test; Fig. 4 *G* and *H*) and an increase in the coefficient of variance (CV) of IPSC amplitudes ($P < 0.03$, t test; Fig. 4 *I* and *J*), suggesting presynaptic expression. Thus, functional CB1 is expressed at presynaptic terminals of tdT-to-tdT unitary synapses but is not regulated by depolarization of postsynaptic FSIs, likely due to the lack of endocannabinoid release.

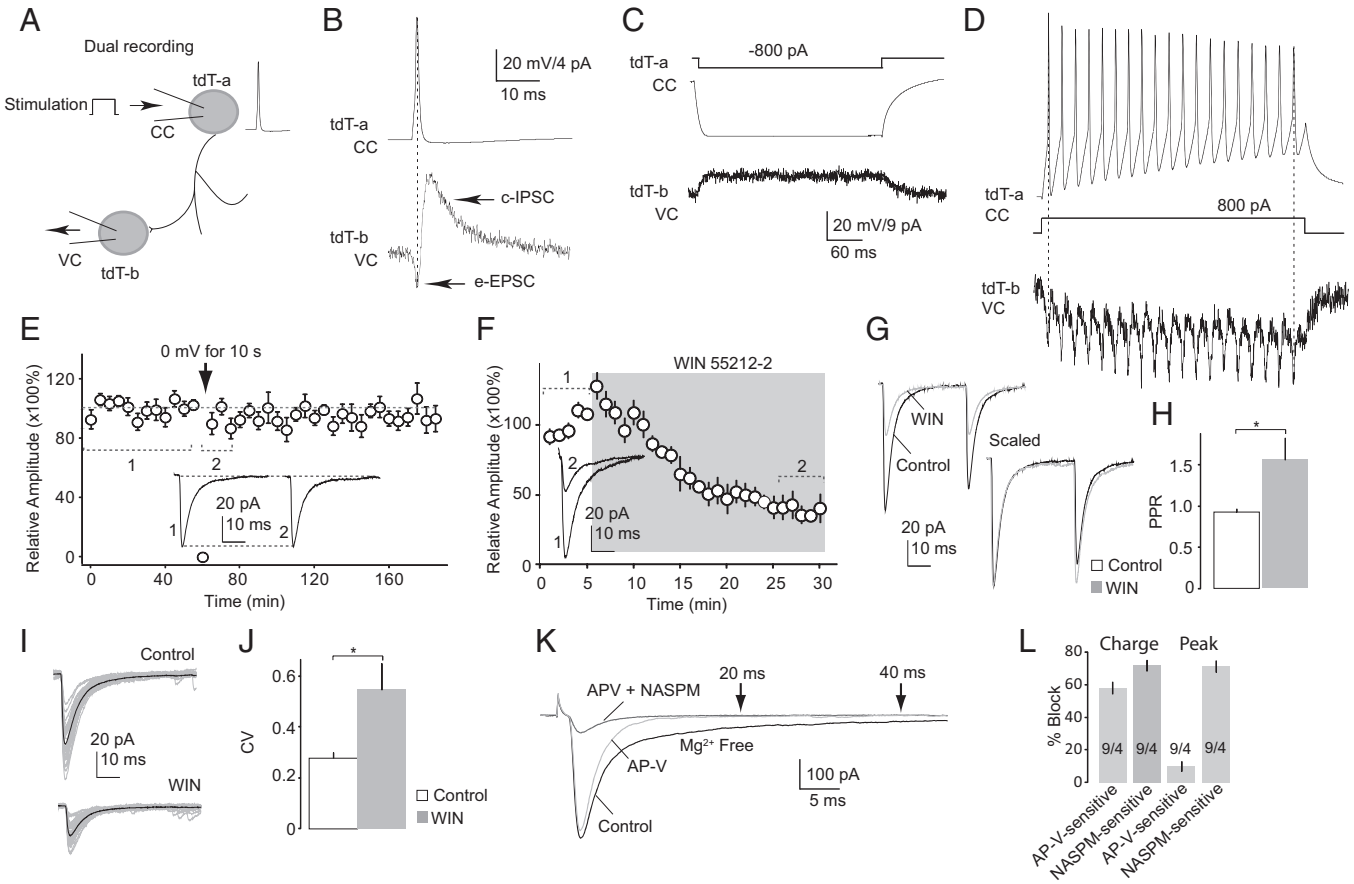

Fig. 4. Synaptic properties of CB1-expressing FSIs. (*A*) Diagram illustrates the experimental setup for dual recording of two tdT-positive FSIs. The first neuron (tdT-a) was recorded in current-clamp (CC) mode, and the second (tdT-b) was recorded in voltage-clamp (VC) mode. (*B*) Example traces show that a single AP in tdT-a elicited a simultaneous inward current (EPSC) in tdT-b, presumably mediated by electrical synapses (e-EPSC). These e-EPSCs in tdT-b were followed by a slow outward current (IPSC) with a delayed onset, presumably mediated by chemical synapses (c-IPSC). Both cells were recorded with K^+-based internal and NBQX (2,3-Dioxo-6-nitro-1,2,3,4-tetrahydrobenzo[f]quinoxaline-7-sulfonamide; 5 μM) in bath. (*C* and *D*) Electrical coupling between tdT-positive FSIs. (*C*) Sustained hyperpolarization of the membrane potential (in current-clamp mode) in tdT-a induced a sustained and temporally correlated outward current (in voltage-clamp mode) in tdT-b. (*D*) Train of repetitive AP firing in tdT-a induced a train of temporally correlated inward currents in tdT-b. These contingent events suggest an electrical coupling between the two recorded neurons. Postsynaptic cell patched with high Cl^- cesium (Cs)-based internal and NBQX (5 μM) in bath. (*E*) Summarized results show a lack of DSI of IPSCs from inhibitory synapses between two tdT-positive FSIs. (*Inset*) Example IPSCs before and after induction of DSI (1 and 2 indicate the positions where traces were taken for averaged data). (*F*) Summarized results show that IPSCs from inhibitory synapses between two tdT-positive FSIs were sensitive to activation of CB1; perfusion of the CB1-selective agonist WIN 55212-2 (5 μM) decreased the amplitude of IPSCs. (*Inset*) Example IPSCs before and after perfusion of WIN 55212-2 (1 and 2 indicate the positions where the averaged traces were taken). Example IPSCs (*G*) and summarized results (*H*) show that the PPR of IPSCs at inhibitory synapses between two tdT-positive FSIs was increased during perfusion of WIN 55212-2 (WIN). (*I*) Thirty consecutive IPSCs (gray) and the average of these IPSCs (black) from an example dual recording of tdT-to-tdT inhibitory synaptic transmission. (*J*) Summarized results show that the CV of IPSCs at inhibitory synapses between two tdT-positive FSIs was increased during perfusion of WIN 55212-2. (*K*) Example averaged evoked EPSCs in a tdT-positive FSI in magnesium-free artificial cerebral spinal fluid (ACSF) with picrotoxin (0.1 mM), in the presence of APV [D-(-)-2-Amino-5-phosphonopentanoic acid; 50 μM] and in the presence of APV and NASPM (1-Naphthyl acetyl spermine trihydrochloride; 200 μM). (*L*) Summarized results show percentage of the integrated EPSC area and peak amplitudes sensitive to APV and NASPM in tdT-positive FSIs. $*P < 0.05$.

Beyond tdT-to-tdT unitary inhibitory synapses, tdT-positive FSIs received extensive excitatory inputs. These excitatory synapses exhibited different properties from excitatory synapses on MSNs. In tdT-positive neurons from the NAc shell, AMPA [2-amino-3-(5-methyl-3-oxo-1,2- oxazol-4-yl)propanoic acid] receptor (AMPAR)-mediated EPSCs were mostly composed of a NASPM (1-Naphthyl acetyl spermine trihydrochloride)-sensitive component, presumably mediated by GluA2-lacking AMPARs (area: 71.7 ± 3.3%, n = 9/4; Fig. 4 *K* and *L* and *SI Results*), which was not typically observed at excitatory synapses in MSNs (33, 34). Moreover, a clear D-(-)-2-Amino-5-phosphonopentanoic acid (APV)-sensitive, N-Methyl-D-aspartate receptor (NMDAR)-mediated component was also present (area: 58.0 ± 3.7%; Fig. 4 *K* and *L* and *SI Results*). These properties of excitatory synapses in NAc tdT-positive FSIs are partially consistent with those in striatal FSIs (20).

Synaptic Transmission from tdT-Positive FSIs to MSNs: Effect of Cocaine Exposure. Paired recording (Fig. 5*A*) in the NAc shell showed that tdT-positive FSIs directly innervated adjacent MSNs in the NAc shell. As shown in Fig. 5*B*, a single AP in tdT-positive neurons elicited a postsynaptic current, with a short delay (0.57 ± 0.06 ms, n = 24) and picrotoxin sensitivity (0.1 mM, n = 4), suggesting that they were unitary IPSCs (uIPSCs).

The NAc is a critical brain region, where exposure to cocaine triggers addiction-related neural adaptations (35, 36). Although the effects of cocaine exposure on NAc principal neurons have been extensively characterized, little is known about how cocaine exposure regulates FSIs, which impose extensive regulation on the principal neurons. Our results show that unitary synaptic transmission from tdT-positive FSIs to MSNs in the NAc did not appear to be altered by repeated exposure to cocaine (15 $mg \cdot kg^{-1} \cdot d^{-1}$, 5 d, at 1 or 40 d of withdrawal). First, the PPR was

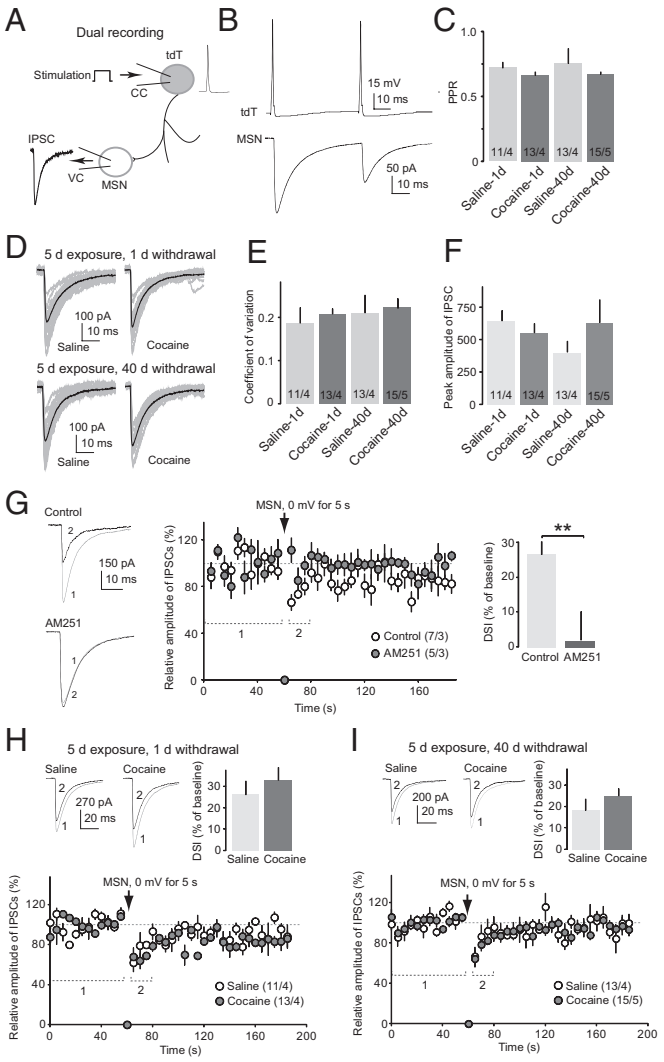

Fig. 5. Unitary synaptic transmission from CB1-expressing FSIs to MSNs in the NAc. (*A*) Diagram illustrates the experimental setup for dual recording of a tdT-positive FSI (tdT) and an MSN in the NAc. The tdT FSI was recorded in current-clamp (CC) mode, and the MSN was recorded in voltage-clamp (VC) mode. (*B*) Example traces show that paired APs (interpulse interval = 50 ms) in a tdT FSI elicited paired uIPSCs in the postsynaptic MSN. (*C*) Summary shows that the PPR of uIPSCs at tdT-to-MSN synapses was not altered on withdrawal day 1 or 40 following repeated exposure to cocaine. (*D*) Examples show 20 consecutive (gray) and averaged uIPSCs (black) at tdT-to-MSN synapses from animals treated with saline or cocaine at 1 or 40 d of withdrawal. (*E*) Summary shows that the CV of uIPSCs at tdT-to-MSN synapses was not significantly altered on withdrawal day 1 or 40 following exposure to cocaine. (*F*) Summary shows that the peak amplitude of uIPSCs at tdT-to-MSN synapses was not significantly altered on withdrawal day 1 or 40 following exposure to cocaine. (*G*) Example averaged traces (*Left*) and summarized results (*Center*) show that DSI was readily induced in uIPSCs at tdT-to-MSN synapses and was prevented by AM251 (2 μM), a CB1-selective inverse agonist (*Right*). The bar graph shows the percentage of reduction from baseline for the first three sweeps (15 s) following the stimulation. Example traces and summarized results show intact DSI of uIPSCs at tdT-to-MSN synapses in animals on withdrawal day 1 (*H*) and day 40 (*I*) after exposure to cocaine. $^{**}P < 0.01$.

not significantly altered in recorded uIPSCs at 1 or 40 d of withdrawal (day 1, $P = 0.28$; day 40, $P = 0.42$, *t* test; Fig. 5 *B* and *C*). Second, the peak amplitude of uIPSCs in MSNs was not significantly altered (day 1, $P = 0.40$; day 40, $P = 0.32$; *t* test; Fig. 5*F*). Third, the amplitude of uIPSCs fluctuated over a trial, and this fluctuation, which could be experimentally assessed by the CV, corresponds to the number of functionally active synapses being activated during transmission. The CV of uIPSCs was not significantly altered either (day 1, $P = 0.59$; day 40, $P = 0.82$, *t* test; Fig. 5 *D* and *E*). Thus, potential cocaine-induced alterations in the number of active synapses per FSI-to-MSN pair were not detected. Fourth, the unitary synaptic transmission from tdT-positive FSIs to MSNs exhibited robust CB1-dependent DSI (induced by a 5-s depolarization of the postsynaptic MSN to 0 mV; 26.7 ± 3.7%), which was blocked by AM 251 (2 μM), an inverse agonist of CB1 ($P = 0.01$, *t* test; Fig. 5*G*). This DSI was not different between saline- and cocaine-administered animals on withdrawal day 1 ($P = 0.46$, *t* test; Fig. 5*H*) or withdrawal day 40 ($P = 0.30$, *t* test; Fig. 5*I*). In addition, other kinetic parameters (e.g., decay time constant, rise time, half-width of uIPSCs) were not altered (Table S2).

Cocaine-Induced Adaptations in CB1-Expressing FSIs. We next examined the impact of cocaine exposure on the intrinsic membrane excitability and synaptic properties of tdT-positive FSIs in the NAc shell. The membrane excitability was assessed by the frequency of evoked APs (24, 37, 38). After 1 d of withdrawal from repeated cocaine administration, the membrane excitability of tdT-positive FSIs was significantly increased [$F_{(1,160)} = 28.77$, $P < 0.001$, two-factor ANOVA; Fig. 6 *A* and *B*], and it remained high on withdrawal day 40 [$F_{(1,160)} = 64.99$, $P < 0.001$, two-factor ANOVA; Fig. 6 *C* and *D*]. This cocaine-induced increase was accompanied by alterations of either the threshold of APs ($P = 0.03$, *t* test; Table S3) or membrane resistance ($P = 0.05$, *t* test; Table S3). Note that the membrane excitability of MSNs in the NAc is decreased during withdrawal from repeated exposure to cocaine (24, 37, 38). Thus, exposure to cocaine differentially regulates principal MSNs and FSIs. Also note that the kinetics of APs in CB1/tdT-expressing FSIs were not altered following exposure to cocaine (Table S3).

In addition to membrane excitability, synaptic input affects the output of FSIs, which, in turn, may regulate the overall output of the NAc. We next examined the potential effects of cocaine on synaptic transmission to tdT-positive FSIs by measuring miniature EPSCs (mEPSCs) and miniature IPSCs (mIPSCs). Neither the mean frequency (cocaine vs. saline: mEPSCs: d 1, $P = 0.21$; d 40, $P = 0.93$; mIPSCs: d 1, $P = 0.49$; d 40, $P = 0.87$; *t* test) nor the mean amplitude (cocaine vs. saline: mEPSCs: d 1, $P = 0.61$; d 40, $P = 0.24$; mIPSCs: d 1, $P = 0.35$; 40 d, $P = 0.63$; *t* test) of mEPSCs or mIPSCs in tdT-positive FSIs was significantly altered on withdrawal day 1 or 40 (Fig. 6 *E*–*L*). Thus, potential cocaine-induced alterations in synaptic inputs to tdT-positive FSIs were not detected. These results, taken together with our earlier results, depict a general picture of the output of the NAc following exposure to cocaine. Because the basal synaptic inputs to tdT-positive FSIs (Fig. 6) and the unitary synaptic transmission from tdT-positive FSIs to MSNs were not altered (Fig. 5), the increased membrane excitability of FSIs (Fig. 6) may readily result in increased inhibitory control of MSNs. This enhanced inhibitory control, together with the "direct" inhibitory effect of cocaine on the membrane excitability of MSNs (24, 37, 38), may substantially suppress the output of NAc MSNs following cocaine exposure.

Discussion

CB1-Expressing Neurons in the NAc. CB1 is one of the most abundant G protein-coupled receptors in the brain (4). In the striatum, the distribution of CB1-expressing neurons exhibits a progressive dorsolateral-to-ventromedial reduction (4) (Fig. 1), with much fewer CB1-positive neurons in the NAc (4, 10, 11, 25). Based on such a low density of expression and certain behavioral patterns induced by intra-NAc manipulation of CB1 signaling, it had been hypothesized that CB1-expressing neurons in the NAc are interneurons (8, 25). Using a genetic marker combined with

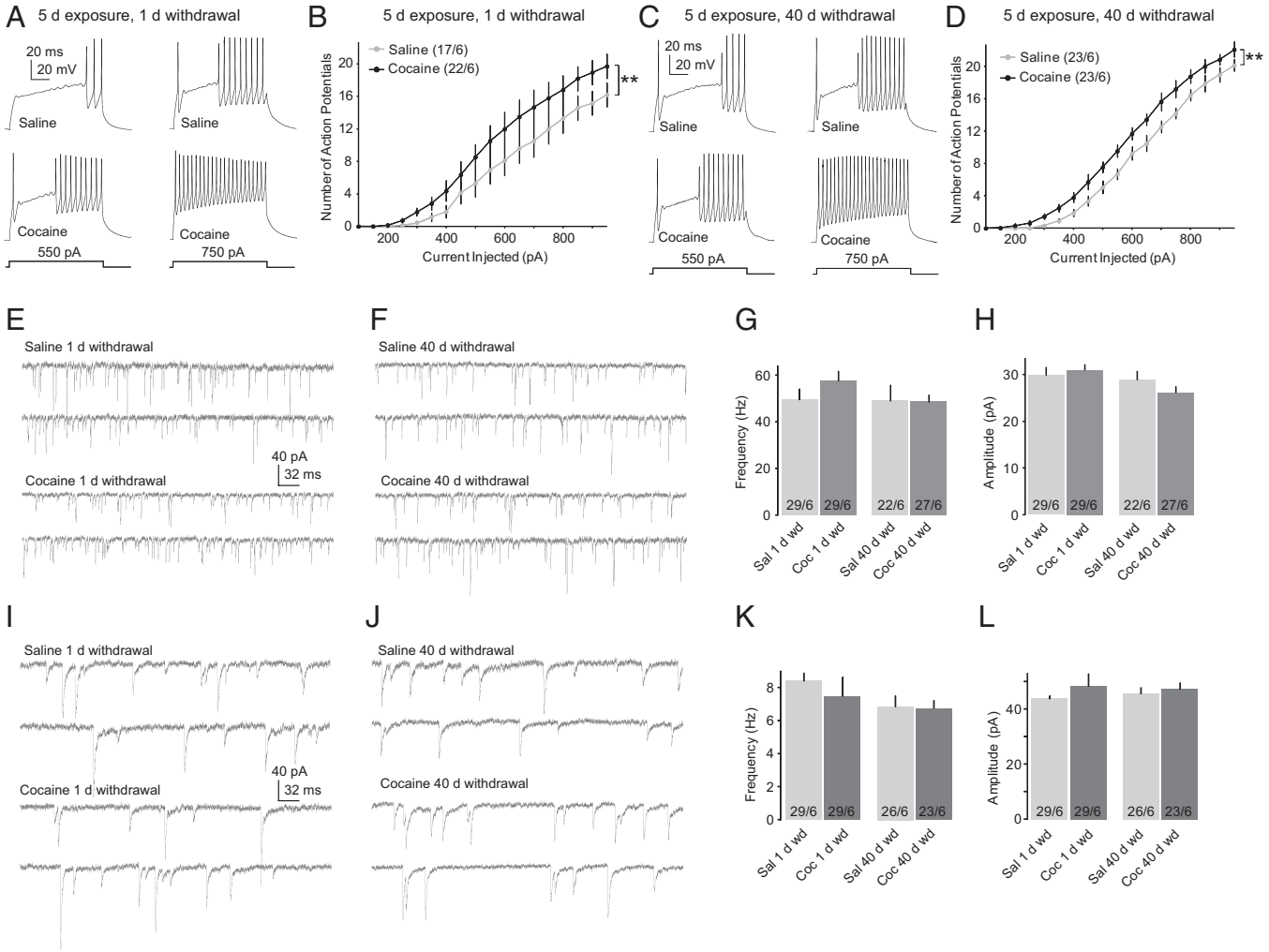

Fig. 6. Exposure to cocaine increased the intrinsic membrane excitability of CB1-expressing FSIs in the NAc. (*A*) Evoked AP firings from example tdT-positive FSIs in the NAc shell from animals on withdrawal day 1 from exposure to saline or cocaine. (*B*) Summarized results show increased membrane excitability of tdT-positive FSIs in the NAc shell on withdrawal day 1 from exposure to cocaine. (*C*) Evoked AP firings from example tdT-positive FSIs in the NAc shell from animals on withdrawal day 40 from exposure to saline or cocaine. (*D*) Summarized results show increased membrane excitability of tdT-positive FSIs in the NAc shell on withdrawal day 40 from exposure to cocaine. (*E*) Example mEPSCs in tdT-positive FSIs from mice with 1 d of withdrawal from saline or cocaine administration. (*F*) Example mEPSCs in tdT-positive FSIs from mice with 40 d of withdrawal from saline or cocaine administration. (*G*) Summarized results show that the frequency of mEPSCs in tdT-positive FSIs was not altered after 1 or 40 d of withdrawal from cocaine (Coc) administration. Sal, saline. (*H*) Summarized results show that the amplitude of mEPSCs in tdT-positive FSIs was not altered after 1 or 40 d of withdrawal from cocaine administration. (*I*) Example mIPSCs in tdT-positive FSIs from mice with 1 d of withdrawal from saline or cocaine administration. (*J*) Example mIPSCs in tdT-positive FSIs from mice with 40 d of withdrawal from saline or cocaine administration. (*K*) Summarized results show that the frequency of mIPSCs in tdT-positive FSIs was not altered after 1 or 40 d of withdrawal from cocaine administration. (*L*) Summarized results show that the amplitude of mIPSCs in tdT-positive FSIs was not altered after 1 or 40 d of withdrawal from cocaine administration. $^{**}P < 0.01$.

electrophysiological recording and immunohistostaining, our current study provides unambiguous evidence that unlike the dorsal striatum, where CB1 is expressed highly in both MSNs and interneurons, NAc CB1 reporter tdT-expressing neurons are exclusively FSIs (Figs. 2 and 3). This result, together with other related observations, provides several important theoretical deductions.

First, given that the primary function of CB1 is to regulate presynaptic release of neurotransmitters (39), the lack of expression in NAc MSNs suggests that synaptic projections from the NAc are not influenced by CB1 signaling. This is important in understanding NAc-originated projections, particularly the projection to the VTA, a key feedback pathway in the brain reward circuit. Our results suggest that this feedback pathway is free of CB1-mediated regulation, because neither the VTA nor the NAc projection neurons express CB1. Thus, although some inhibitory presynaptic terminals in the VTA carry CB1 (6) (Fig. 1*D* and Fig. S1), which may underlie CB1-mediated modulation of these synapses (40–42), these inhibitory synapses on VTA neurons are not likely projected from the NAc based on our present results. In addition, although CB1-mediated regulation of VTA-to-NAc dopamine release has been observed (43), because VTA dopamine neurons do not express CB1 (12) (Fig. 1*D* and Fig. S1 *D* and *E*), the VTA-to-NAc presynaptic dopaminergic terminals are also not likely regulated by CB1 signaling directly. As such, there seems no within-circuit presynaptic CB1-mediated regulation through the entire VTA (dopamine)-NAc-VTA loop. If so, CB1-mediated regulation of dopamine release to the NAc (43, 44) must be mediated by other CB1-expressing projections.

Second, NAc neurons are thought to be organized as separate functional ensembles (45). Our results suggest that adjacent CB1-expressing FSIs were often connected to each other with

both electrical and chemical synapses (Fig. 4). Illuminated primarily by the studies of striatal FSIs (19, 20, 46–51), these CB1-expressing FSIs may provide feed-forward inhibition of NAc MSNs, with high timing and anatomical specificities. Thus, the electrical coupling between CB1-expressing FSIs may serve as one type of organizer to synchronize the functional output of a small group of MSNs (ensemble).

Third, approximately half of PV-positive neurons did not express CB1 (Fig. 3 *A–D*). Assuming that most PV-positive neurons in the NAc are FSIs and exhibit electrical coupling as demonstrated in the striatum, only approximately half of FSIs and their controlled ensembles would be sensitive to CB1-mediated modulation. This potential dichotomy raises several intriguing questions for future studies: (*i*) Are these CB1 ensembles those that mediate cannabinoid-elicited emotional and motivational alterations? (*ii*) If so, how do these CB1 ensembles interact with other non-CB1 ensembles? (*iii*) Can these CB1 ensembles be selectively targeted to achieve therapeutic specificity?

Fourth, because CB1/FSIs only partially overlap with PV-expressing neurons, previous studies using PV as a marker to assess the number of FSIs in the NAc/striatum may underestimate the total number of FSIs by ∼50%. This is anecdotally supported by the unexpectedly high frequency of encountering FSIs during random sampling of striatal neurons in brain slices (19) and in vivo (52). Furthermore, using both CB1 and PV as markers for FSIs, our estimated spacing between FSIs was ∼122 μm (*SI Results*), a distance that is within the axonal arbor of FSIs (18). This estimated anatomical setup suggests extensive control of the MSN population by FSIs.

Effects of Cocaine. An important finding of the present study is that following cocaine exposure, the intrinsic membrane excitability of CB1-expressing FSIs was increased, whereas the synaptic efficacy of FSI-to-MSN transmission appeared to remain unaltered (Figs. 5 and 6). In the striatum, and also likely in the NAc, FSIs exert strong inhibitory control on the output MSNs. Our previous results show that the membrane excitability of MSNs is decreased following contingent or noncontingent exposure to cocaine (24, 37, 38). Thus, the effects of cocaine on CB1-expressing FSIs may increase the inhibitory influence over MSNs, further decreasing the membrane responsiveness of the NAc to excitatory input during cocaine withdrawal. As such, the increased membrane excitability of CB1-expressing FSIs during cocaine withdrawal (Fig. 6) provides a circuitry mechanism to dampen further the responsiveness of the NAc to excitatory input. Beyond the level of individual MSNs, cocaine's effect on CB1-expressing FSIs can also exert an impact at the functional ensemble level. Because one CB1-expressing FSI may simultaneously influence an ensemble of NAc MSNs, the cellular behaviors of such a putative functional ensemble can be, to some extent, synchronized toward the same functional mode shaped by the effect of cocaine on FSIs. Collectively, our results suggest that the effects of cocaine on CB1-expressing FSIs and MSNs coordinate to decrease the functional responsiveness of NAc MSNs to excitatory input.

However, the excitatory synaptic input to MSNs in the NAc is also, per se, subject to cocaine-induced adaptation. During cocaine withdrawal, the postsynaptic responsiveness (number of postsynaptic AMPARs) of excitatory synaptic input to NAc MSNs is increased (36), functionally opposing the effects of cocaine on the membrane excitability of MSNs and FSIs. These opposing effects do not simply cancel out each other or follow a linear integration; rather, they may reshape the input-output equation of NAc MSNs, as implied by a previous computational model (38). Specifically, the decreased membrane responsiveness during cocaine withdrawal may effectively prevent AP firing of NAc MSNs in response to low-intensity excitatory synaptic inputs that otherwise elicit APs in naive animals. These low-intensity excitatory inputs may represent basal or background stimulation, such as stimuli associated with the home cages where animals dwell. On high-intensity excitatory inputs, which can be produced by reexposure to cocaine or cocaine-associated cues during withdrawal, the effect of cocaine on excitatory synaptic strength would predominate, resulting in a higher level of AP firing in NAc MSNs than in naive animals (38). This speculation is supported by observations of hypoactivity of the NAc during cocaine withdrawal and hyperactivity of NAc on reexposure to cocaine after withdrawal (53, 54).

In summary, the present study characterized the biochemical and biophysical properties of CB1-expressing neurons in the NAc and demonstrated cocaine-induced adaptations in these neurons. These results suggest that NAc CB1-expressing FSIs may serve as critical neuronal targets for cocaine to induce cellular and behavioral alterations related to addiction.

Experimental Procedures

Experimental procedures are provided in *SI Experimental Procedures*. These procedures include generation of the CB1-tdT mouse line. Other sections included are experimental animals and cocaine administration; immunohistochemistry, imaging, and biochemistry; slice preparation and electrophysiology; and data analysis.

ACKNOWLEDGMENTS. We thank Drs. R. Y. Tsien and M. R. Capecchi for DNA constructs and the Max-Planck-Institute for Experimental Medicine animal and DNA core facilities for blastocyte injections, primer synthesis, and DNA sequencing. The study was supported by the American Heart Association, the Humboldt Foundation, the German Science Foundation through the CNMPB, and National Institutes of Health–National Institute on Drug Abuse Grants DA029565, DA028020, DA023206 and DA024570, and DA031551. The European Neuroscience Institute is jointly funded by the University Medicine Göttingen and the Max Planck Society.

1. Gardner EL (2005) Endocannabinoid signaling system and brain reward: Emphasis on dopamine. *Pharmacol Biochem Behav* 81:263–284.
2. Maldonado R, Valverde O, Berrendero F (2006) Involvement of the endocannabinoid system in drug addiction. *Trends Neurosci* 29:225–232.
3. Arnold JC (2005) The role of endocannabinoid transmission in cocaine addiction. *Pharmacol Biochem Behav* 81:396–406.
4. Herkenham M, et al. (1990) Cannabinoid receptor localization in brain. *Proc Natl Acad Sci USA* 87:1932–1936.
5. Marsicano G, Lutz B (1999) Expression of the cannabinoid receptor CB1 in distinct neuronal subpopulations in the adult mouse forebrain. *Eur J Neurosci* 11:4213–4225.
6. Mátyás F, et al. (2006) Subcellular localization of type 1 cannabinoid receptors in the rat basal ganglia. *Neuroscience* 137:337–361.
7. Ramiro-Fuentes S, Ortiz O, Moratalla R, Fernandez-Espejo E (2010) Intra-accumbens rimonabant is rewarding but induces aversion to cocaine in cocaine-treated rats, as does in vivo accumbal cannabinoid CB1 receptor silencing: Critical role for glutamate receptors. *Neuroscience* 167:205–215.
8. Morra JT, Glick SD, Cheer JF (2010) Neural encoding of psychomotor activation in the nucleus accumbens core, but not the shell, requires cannabinoid receptor signaling. *J Neurosci* 30:5102–5107.
9. Deshmukh S, et al. (2007) Postnatal development of cannabinoid receptor type 1 expression in rodent somatosensory cortex. *Neuroscience* 145:279–287.
10. Mailleux P, Vanderhaeghen JJ (1992) Distribution of neuronal cannabinoid receptor in the adult rat brain: A comparative receptor binding radioautography and in situ hybridization histochemistry. *Neuroscience* 48:655–668.
11. Tsou K, Brown S, Sañudo-Peña MC, Mackie K, Walker JM (1998) Immunohistochemical distribution of cannabinoid CB1 receptors in the rat central nervous system. *Neuroscience* 83:393–411.
12. Julian MD, et al. (2003) Neuroanatomical relationship between type 1 cannabinoid receptors and dopaminergic systems in the rat basal ganglia. *Neuroscience* 119: 309–318.
13. Fusco FR, et al. (2004) Immunolocalization of CB1 receptor in rat striatal neurons: A confocal microscopy study. *Synapse* 53:159–167.
14. Bodor AL, et al. (2005) Endocannabinoid signaling in rat somatosensory cortex: Laminar differences and involvement of specific interneuron types. *J Neurosci* 25: 6845–6856.
15. Wedzony K, Chocyk A (2009) Cannabinoid CB1 receptors in rat medial prefrontal cortex are colocalized with calbindin- but not parvalbumin- and calretinin-positive GABA-ergic neurons. *Pharmacol Rep* 61:1000–1007.

16. Kawamura Y, et al. (2006) The CB1 cannabinoid receptor is the major cannabinoid receptor at excitatory presynaptic sites in the hippocampus and cerebellum. *J Neurosci* 26:2991–3001.
17. Taverna S, Canciani B, Pennartz CM (2007) Membrane properties and synaptic connectivity of fast-spiking interneurons in rat ventral striatum. *Brain Res* 1152: 49–56.
18. Kawaguchi Y (1993) Physiological, morphological, and histochemical characterization of three classes of interneurons in rat neostriatum. *J Neurosci* 13:4908–4923.
19. Koós T, Tepper JM (1999) Inhibitory control of neostriatal projection neurons by GABAergic interneurons. *Nat Neurosci* 2:467–472.
20. Gittis AH, Nelson AB, Thwin MT, Palop JJ, Kreitzer AC (2010) Distinct roles of GABAergic interneurons in the regulation of striatal output pathways. *J Neurosci* 30: 2223–2234.
21. Tepper JM, Tecuapetla F, Koos T, Ibanez-Sandoval O (2010) Heterogeneity and diversity of striatal GABAergic interneurons. *Front Neuroanat* 4(article 150):1–18.
22. Kawaguchi Y, Wilson CJ, Augood SJ, Emson PC (1995) Striatal interneurones: Chemical, physiological and morphological characterization. *Trends Neurosci* 18: 527–535.
23. O'Donnell P, Grace AA (1993) Physiological and morphological properties of accumbens core and shell neurons recorded in vitro. *Synapse* 13:135–160.
24. Dong Y, et al. (2006) CREB modulates excitability of nucleus accumbens neurons. *Nat Neurosci* 9:475–477.
25. Hohmann AG, Herkenham M (2000) Localization of cannabinoid CB(1) receptor mRNA in neuronal subpopulations of rat striatum: A double-label in situ hybridization study. *Synapse* 37:71–80.
26. Katona I, Acsády L, Freund TF (1999) Postsynaptic targets of somatostatin-immunoreactive interneurons in the rat hippocampus. *Neuroscience* 88:37–55.
27. Kubota Y, Kawaguchi Y (2000) Dependence of GABAergic synaptic areas on the interneuron type and target size. *J Neurosci* 20:375–386.
28. Centonze D, et al. (2002) Activation of dopamine D1-like receptors excites LTS interneurons of the striatum. *Eur J Neurosci* 15:2049–2052.
29. Centonze D, et al. (2003) Receptor subtypes involved in the presynaptic and postsynaptic actions of dopamine on striatal interneurons. *J Neurosci* 23:6245–6254.
30. Ibáñez-Sandoval O, et al. (2010) Electrophysiological and morphological characteristics and synaptic connectivity of tyrosine hydroxylase-expressing neurons in adult mouse striatum. *J Neurosci* 30:6999–7016.
31. Bubser M, Scruggs JL, Young CD, Deutch AY (2000) The distribution and origin of the calretinin-containing innervation of the nucleus accumbens of the rat. *Eur J Neurosci* 12:1591–1598.
32. Arlotta P, Molyneaux BJ, Jabaudon D, Yoshida Y, Macklis JD (2008) Ctip2 controls the differentiation of medium spiny neurons and the establishment of the cellular architecture of the striatum. *J Neurosci* 28:622–632.
33. Kourrich S, Rothwell PE, Klug JR, Thomas MJ (2007) Cocaine experience controls bidirectional synaptic plasticity in the nucleus accumbens. *J Neurosci* 27:7921–7928.
34. McCutcheon JE, Wang X, Tseng KY, Wolf ME, Marinelli M (2011) Calcium-permeable AMPA receptors are present in nucleus accumbens synapses after prolonged withdrawal from cocaine self-administration but not experimenter-administered cocaine. *J Neurosci* 31:5737–5743.
35. Koob GF, Volkow ND (2010) Neurocircuitry of addiction. *Neuropsychopharmacology* 35:217–238.
36. Wolf ME (2010) The Bermuda Triangle of cocaine-induced neuroadaptations. *Trends Neurosci* 33:391–398.
37. Ishikawa M, et al. (2009) Homeostatic synapse-driven membrane plasticity in nucleus accumbens neurons. *J Neurosci* 29:5820–5831.
38. Mu P, et al. (2010) Exposure to cocaine dynamically regulates the intrinsic membrane excitability of nucleus accumbens neurons. *J Neurosci* 30:3689–3699.
39. Chevaleyre V, Takahashi KA, Castillo PE (2006) Endocannabinoid-mediated synaptic plasticity in the CNS. *Annu Rev Neurosci* 29:37–76.
40. Szabo B, Siemes S, Wallmichrath I (2002) Inhibition of GABAergic neurotransmission in the ventral tegmental area by cannabinoids. *Eur J Neurosci* 15:2057–2061.
41. Riegel AC, Lupica CR (2004) Independent presynaptic and postsynaptic mechanisms regulate endocannabinoid signaling at multiple synapses in the ventral tegmental area. *J Neurosci* 24:11070–11078.
42. Pan B, Hillard CJ, Liu QS (2008) Endocannabinoid signaling mediates cocaine-induced inhibitory synaptic plasticity in midbrain dopamine neurons. *J Neurosci* 28:1385–1397.
43. Lupica CR, Riegel AC (2005) Endocannabinoid release from midbrain dopamine neurons: A potential substrate for cannabinoid receptor antagonist treatment of addiction. *Neuropharmacology* 48:1105–1116.
44. Cheer JF, Wassum KM, Heien ML, Phillips PE, Wightman RM (2004) Cannabinoids enhance subsecond dopamine release in the nucleus accumbens of awake rats. *J Neurosci* 24:4393–4400.
45. Pennartz CM, Groenewegen HJ, Lopes da Silva FH (1994) The nucleus accumbens as a complex of functionally distinct neuronal ensembles: An integration of behavioural, electrophysiological and anatomical data. *Prog Neurobiol* 42:719–761.
46. Berke JD, Okatan M, Skurski J, Eichenbaum HB (2004) Oscillatory entrainment of striatal neurons in freely moving rats. *Neuron* 43:883–896.
47. Tepper JM, Bolam JP (2004) Functional diversity and specificity of neostriatal interneurons. *Curr Opin Neurobiol* 14:685–692.
48. Wilson CJ, Weyrick A, Terman D, Hallworth NE, Bevan MD (2004) A model of reverse spike frequency adaptation and repetitive firing of subthalamic nucleus neurons. *J Neurophysiol* 91:1963–1980.
49. Berke JD (2008) Uncoordinated firing rate changes of striatal fast-spiking interneurons during behavioral task performance. *J Neurosci* 28:10075–10080.
50. Gruber AJ, Powell EM, O'Donnell P (2009) Cortically activated interneurons shape spatial aspects of cortico-accumbens processing. *J Neurophysiol* 101:1876–1882.
51. Lansink CS, Goltstein PM, Lankelma JV, Pennartz CM (2010) Fast-spiking interneurons of the rat ventral striatum: Temporal coordination of activity with principal cells and responsiveness to reward. *Eur J Neurosci* 32:494–508.
52. Berke JD (2009) Fast oscillations in cortical-striatal networks switch frequency following rewarding events and stimulant drugs. *Eur J Neurosci* 30:848–859.
53. Febo M, et al. (2005) The neural consequences of repeated cocaine exposure revealed by functional MRI in awake rats. *Neuropsychopharmacology* 30:936–943.
54. Peoples LL, Kravitz AV, Guillem K (2007) The role of accumbal hypoactivity in cocaine addiction. *ScientificWorldJournal* 7:22–45.
55. Paxinos G, Franklin KBJ (2001) *The Mouse Brain in Stereotaxic Coordinates* (Academic, San Diego).